Impact of Patch Welding Repair on the Compressive Strength of Thickness-reduced Steel Members

Feng Jiang[1], Yuxuan Cheng[2], Mikihito Hirohata[3] and Károly Jármai[4]

[1,2,3] Department of Civil Engineering, Osaka University, 2-1 Yamadaoka, Suita 565-0871, Osaka, Japan, f-jiang@civil.eng.osaka-u.ac.jp; y-cheng@civil.eng.osaka-u.ac.jp; hirohata@civil.eng.osaka-u.ac.jp

[4] Faculty of Mechanical Engineering and Informatics, University of Miskolc, H-3515 Miskolc, Hungary, karoly.jarmai@uni-miskolc.hu

Abstract: This study explores the efficacy of patch welding repair in restoring the compressive strength of steel structural members affected by corrosion-induced thickness reduction. Traditionally, high-strength bolts are the preferred method for patch-repairing such damages. However, patch welding presents a viable alternative, offering benefits like light weight and ease of workability. Compression tests were conducted on steel plates with varied degrees of thickness reduction to assess the effects of patch plate dimensions on the compressive behavior of the repaired plates. Additionally, elastic-plastic analysis simulations were performed to scrutinize the behavior of specimens with varying parameters. The findings suggest that to match the compressive strength of undamaged steel plates, the thicknesses of the weld throat and patch plates must be increased by a factor of 1.1 relative to the thickness loss. Moreover, for optimal effectiveness, the length of the patch plate should exceed the affected area by at least 30 mm. This study illuminates the potential of patch welding as a repair technique for corrosion-compromised steel structures.

Keywords: patch welding repair; thickness reduction; compressive strength; FEM

1 Introduction

A significant number of steel structures built before the 1930s continue to function globally. For many years, the number of reports on steel structures with deterioration and damage has been increasing, which are considered to pose public safety risks [1]. Corrosion, the main cause of this deterioration, erodes the surface of steel components, reducing their cross-sectional areas, structural integrity, and load-bearing capacity [2]. Economically, corrosion-related damage accounts for estimated losses of 3-5% of the gross national product in industrialized nations [3].

Recognizing the need for repair and reinforcement of these structures is crucial for infrastructure maintenance and to extend their lifespan [4]. Therefore, various repair and reinforcement methods have been developed for corroded steel members, generally involving the addition of new materials to the compromised areas. Steel plates are favored for these repairs due to their ease of use, effectiveness, and cost-efficiency [5]. While Carbon Fiber Reinforced Polymer (CFRP) is increasingly used for lightweight, high-strength repairs, it performs poorly on uneven, corroded surfaces and cannot restore highly corroded structures to their original condition [6, 7]. Therefore, steel plates remain the predominant choice for patch repairs.

There are three primary methods for attaching steel patch plates: bolting, adhesives, and welding. Bolting is preferred for its reliability and simplicity, but requires drilling in non-corroded areas, adding weight and often necessitating large machinery which complicates repairs at bridge girder ends [8]. Adhesives offer a lightweight, no-drill application, but have durability issues, particularly under moisture conditions that weaken joints in structures like bridges [9]. Consequently, adhesives are seldom used as the sole method in patch plate repairs. Welding, less frequently employed than bolting or adhesives, can lead to stress concentrations, local deformations, and residual stresses [10, 11]. The weldment between the base and patch plates may initiate fatigue cracks post-repair [12]. Additionally, welding can be hazardous and necessitates halting certain processes for safety reasons, incurring additional costs [13, 14]. However, welding offers unique advantages, addressing some of the shortcomings of other methods. It avoids increased structural weight since it requires no drilling and can be executed in confined spaces [15]. These attributes make welding a compelling alternative for patch repairs, particularly at girder ends.

This paper notes welding as an effective method for patch repairing corroded steel structures, particularly in narrow, moist areas at girder ends. Although previous studies have mainly examined mechanical properties and overall effectiveness of patch welding [16], there's been little empirical research on how factors like patch plate size and weld bead size affect load capacity recovery. This study fills this gap by exploring different weld-patch sizes on plates with varied corrosion-induced thickness reductions. It uses a uniform thickness reduction model to simplify the complex surface profiles typically caused by corrosion. Through adjusting the weld bead size, and the patch plate's length and thickness, the study aims to measure maximum stress levels and compressive behavior. It combines experimental and simulation techniques to validate repair outcomes, striving to develop a guideline for determining optimal weld-patch sizes for practical applications.

2 Experiment

2.1 Specimens

Static monotonic compression tests were carried out on steel plates that had been thinned and repaired through patch welding. Corrosion typically occurs beneath deck expansion joints, leading to severe localized damage [17]. The tests used specimens that replicated these conditions, as shown in Figure 1. Details of the specimens are listed in Table 1. Eighteen specimens, divided into six types (A to F), were tested. Each type was based on a SM400A steel plate, standardized by JIS, measuring 600 mm in length, 18 mm in thickness, and 40 mm in width. To mimic corrosion, 4.5 mm was milled from both sides of the central section, leaving a thinned middle of 9 mm. Each type varied in patch plate dimensions and weld bead sizes, with three specimens per type.

Patch plates of SM400A steel, in 4.5 mm and 7.5 mm thicknesses, were used for repair. The base plate's central section was thinned, followed by surface treatments: blasting the base and milling the patch plates to remove scale. These plates were then fillet welded to the base edges using gas metal arc welding, with parameters set to 140 A for a 4.5 mm bead and 180 A for a 7.5 mm bead, 25 V voltage, and a welding speed of 1.2 mm/s. The welding wire complied with JIS Z 3316, W49A3U16 standards. Table 2 outlines the chemical and mechanical properties of the materials used. The study simulated a severe corrosion scenario by halving the base plate thickness from 18 mm to 9 mm, reflecting prior findings of up to 50% cross-sectional reduction in bridge beams due to corrosion [18]. The study focuses on this extreme case, with additional scenarios discussed in Section 3.4.

Figure 1 illustrates the variables of specimens including t_b (base plate thickness), d_c (thickness reduction), r (range of thickness reduction), L (length of patch plate), t_p (thickness of patch plate), s (weld bead size), and t_w (throat thickness of the weld bead). For effective static stress transfer, the throat thickness of the weld bead, t_w, should exceed the thickness reduction, d_c. For a 4.5 mm thickness reduction on both sides of the base plate, achieving the compressive strength of an unreduced base plate requires a minimum weld bead size, s, of 6.36 mm, since $s / \sqrt{2} = t_w \geq d_c = 4.5$ mm. This experiment used two weld bead sizes, 4.5 mm and 7.5 mm, to explore their impact on repair efficacy. The experiment also varied the patch plate's length (90 mm and 150 mm) and thickness (4.5 mm and 7.5 mm) to fully assess their roles in enhancing the repair's effectiveness.

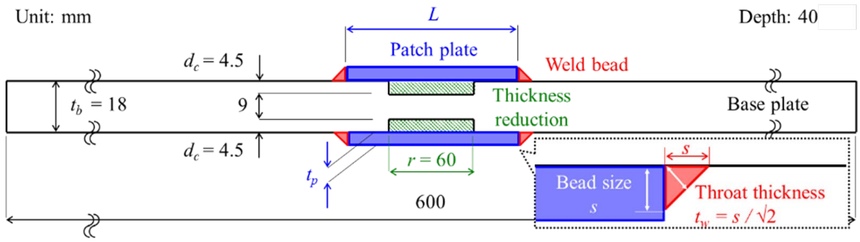

Figure 1
Dimensions and variables of specimens

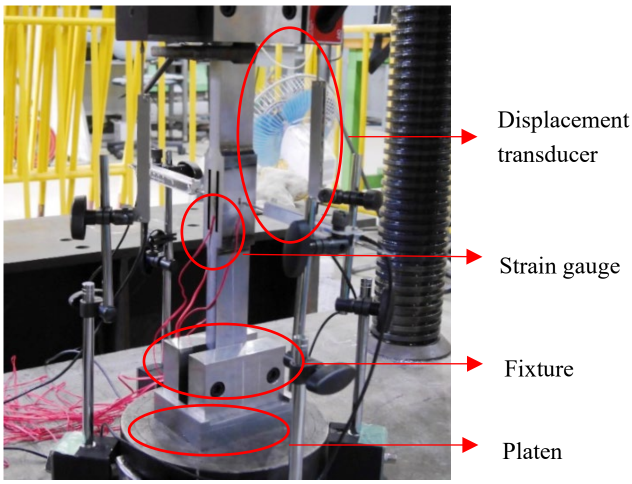

Figure 2
Experimental setup of the compression tests

Table 1
Parameters of specimens

Type (number)	Base plate thickness, t_b	Thickness reduction, d_c	Reduction range, r	Patch plate length, L	Patch plate thickness, t_p	Bead size, s (Throat thickness, t_w)
A (3)	18	4.5	60	90	4.5	4.5 (3.2)
B (3)	18	4.5	60	90	7.5	7.5 (5.3)
C (3)	18	4.5	60	90	7.5	4.5 (3.2)
D (3)	18	4.5	60	150	4.5	4.5 (3.2)
E (3)	18	4.5	60	150	7.5	7.5 (5.3)
F (3)	18	4.5	60	150	7.5	4.5 (3.2)

Table 2
Chemical compositions and mechanical properties of steel materials

	Chemical compositions (mass %)					Mechanical properties		
	C	Si	Mn	P	S	Yield strength (N/mm^2)	Tensile strength (N/mm^2)	Elongation (%)
Base plate (SM400A)	0.07	0.20	0.84	0.016	0.007	290	430	32
Patch plate (SM400A)	0.08	0.25	0.82	0.018	0.003	341	450	31
Weld metal (JIS Z 3316, W49A3U16)	0.09	0.73	1.35	0.009	0.010	480	580	30

2.2 Compression Test

The compression tests were conducted using a universal testing machine equipped with platens and specialized fixtures to apply compressive loads to the specimens. Figure 2 illustrates the experimental setup. To assess the strain distribution underload, strain gauges were affixed to the midspan of both the base and patch plates. These gauges helped confirm that the load applied was uniformly vertical, avoiding any eccentric bending effects. Four displacement transducers were positioned around each specimen: two for measuring vertical displacement and two for horizontal displacement. The two corresponding transducers recorded the average vertical displacement to plot the load-displacement curves. Meanwhile, the differences in horizontal displacements recorded by the remaining two transducers were analyzed to assess the deformation of the patch plates.

A key aspect of this experiment was measuring the maximum load each specimen could bear. The resulting load-displacement curves were then used to evaluate the effectiveness of patch welding repair under different experimental conditions.

2.3 Experimental Results

2.3.1 Load-Displacement Curves

Figure 3 presents photographs of specimens A through F post-compression experiments. The failure of these specimens was predominantly due to excessive plastic deformation caused by static overload. Notably, small cracks were observed at the welding joint of specimen E. Table 3 details the horizontal deformation of the patch plates and base plate at maximum load. Displacement 1 refers to the horizontal displacement at the center of the specimen's more deformed side at maximum load, while Displacement 2 measures the less deformed side. Positive displacement values indicate bending outward, and negative values indicate bending inward. The experimental data revealed that at maximum load, the patch plates and base plates of all specimens typically showed asymmetric deformation: one side experienced more significant deformation than the other, except in the case of specimen E. For specimen E, both sides showed significant deformation at maximum load. This asymmetry in deformation generally suggests that the patch plate effectively restrains bending in the whole structure under static compression. However, the anomalous behavior of specimen E indicates a different bending restraint due to possible welding defects.

Figure 4 displays the load-displacement curves for each specimen. The maximum loads of each curve, their average values, and the standard deviation in percentage (RSD) are also shown in the figures. An operational error with the loading machine resulted in inaccurate displacement data for one of the D specimens; thus, only two results for specimen D are included in the figure. Due to the welding defects in specimen E, which potentially reduce compressive strength, its results are excluded from this discussion and will be analyzed separately in subsequent sections.

The experimental data showed that specimen B, with a 7.5 mm weld bead size, had an average maximum load of 196.45 kN. This value was significantly higher than that of other specimens with a 4.5 mm weld bead size. In instances where the weld bead size was 4.5 mm, and the patch plate length was consistent, but thickness varied (comparing A with C and D with F), the specimens with a 7.5 mm thickness patch plate exhibited a higher maximum load. Moreover, even when both the length and thickness of the patch plate differed (comparing A with F, and C with D), the specimen with a 7.5 mm thickness patch plate still achieved a greater maximum load, regardless of the length of the patch plates. Additionally, when the weld bead size and patch plate thickness were constant, the maximum load for the type with a 90 mm patch plate length was greater than that for the 150 mm length type.

These findings suggest that the three variable parameters – weld bead size, thickness of the patch plate, and length of the patch plate – have a discernible impact on the effectiveness of patch welding repair. However, a more detailed analysis is required to fully understand their specific effects and quantify their significance for practical construction applications. Therefore, a series of simulations were conducted using an elastic-plastic analysis model under various conditions to investigate further the extent of these parameters' influence on repair efficacy.

2.3.2 Specimen E with Welding Defects

Figure 5 reveals that specimens in type E exhibited welding defects, specifically incomplete root fusion or penetration. These defects led to an average reduction of 0.8 mm in the throat thickness of the weld bead. Moreover, the weld bead size in type E was smaller than anticipated, measuring 6 mm instead of the intended 7.5 mm. This discrepancy further decreased the throat thickness. Consequently, the throat thickness in type E was reduced to 3.4 mm, representing a 35.8% decrease from the expected 5.3 mm.

Given these deviations, the actual specifications for specimens in type E were revised to a patch plate length of 150 mm, a patch plate thickness of 7.5 mm, and a weld bead size of 4.9 mm. To assess the impact of these welding defects on the maximum load capacity, a simulation of the compression experiments was conducted for specimen E using an elastic-plastic analysis model, as detailed in section 3.2.

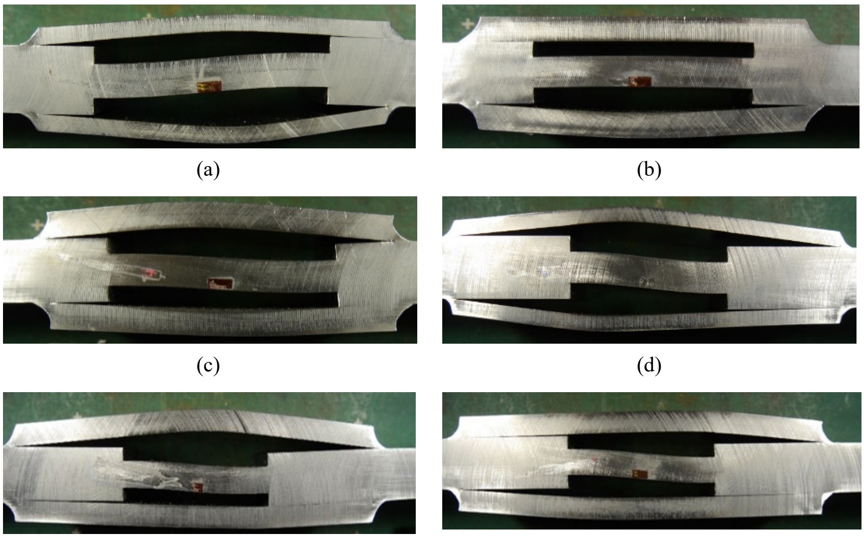

(a) (b) (c) (d) (e) (f)

Figure 3

The pictures of specimens after the compression experiments: (a) Specimen A; (b) Specimen B; (c) Specimen C; (d) Specimen D; (e) Specimen E; (f) Specimen F

Table 3

Horizontal displacement (Dis1, Dis2: mm) of the patch plate at maximum load (Max: kN)

	A1	A2	A3	B1	B2	B3	C1	C2	C3
Max	155.9	149.8	155.9	195.2	196.9	197.3	176.9	184.2	180.2
Dis1	1.201	1.334	0.897	1.209	1.061	0.601	1.115	1.108	0.842
Dis2	0.507	0.211	0.078	0.125	0.172	0.094	0.335	0.218	0.086
	D1	D2	D3	E1	E2	E3	F1	F2	F3
Max	149.2	149.5	-	181.3	170.1	175.4	176.9	178.3	179.9
Dis1	1.076	0.983	-	1.396	1.591	1.997	1.529	1.513	1.739
Dis2	0.585	0.437	-	1.342	1.276	1.217	0.749	0.172	0.725

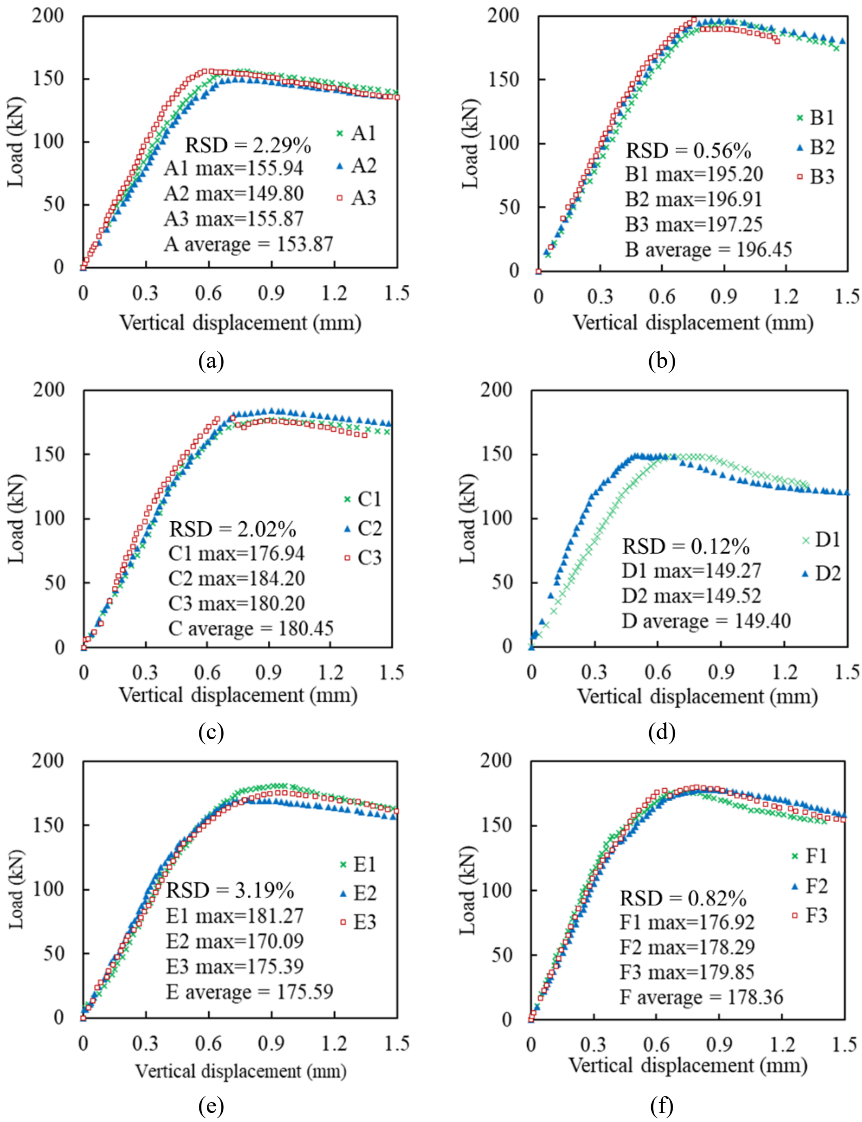

Figure 4
Load-displacement curves: (a) Specimen A; (b) Specimen B; (c) Specimen C; (d) Specimen D; (e) Specimen E; (f) Specimen F

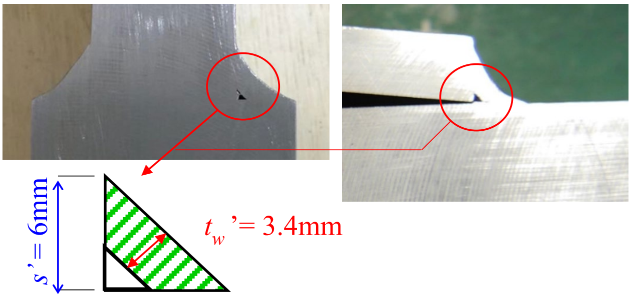

Figure 5
Welding defects on specimen E

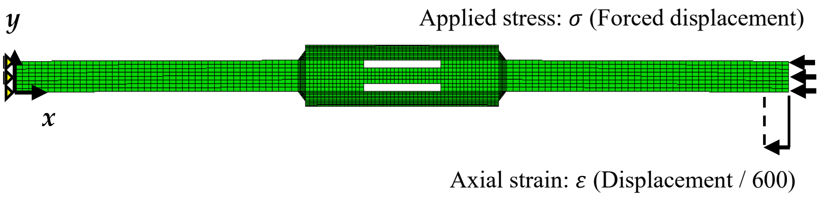

Figure 6
2D elastic-plastic analysis model (e.g. L = 150 mm, t_p = 7.5 mm, s = 4.5 mm)

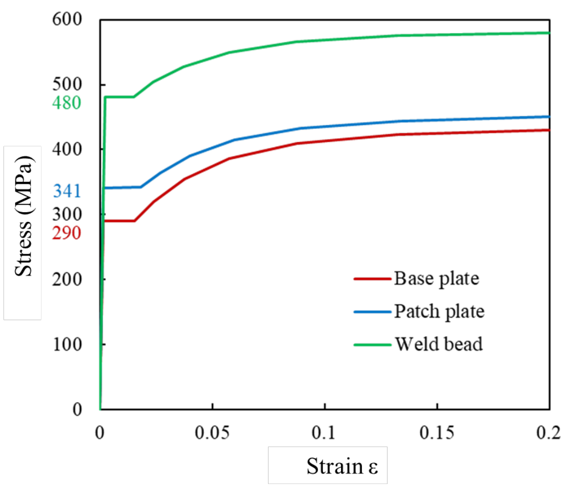

Figure 7
Stress-strain curve of steel materials

3 Simulation

3.1 Analytical Model and Conditions

The finite element analysis software ABAQUS Ver. 6.14 was used for simulating the experiments. A simplified model was adapted to align with the experimental conditions, featuring a uniform and constant thickness reduction on the surface at the model's midpoint. Given the long dimensions and symmetry of the steel members, and considering that the primary deformation under compressive load was bending deformation, the slight deformation in the width direction was deemed negligible. Therefore, a two-dimensional elastic-plastic analysis with plane strain condition was chosen for this simulation.

Figure 6 illustrates the structure and analytical conditions of the model. The model was assembled using 4-node elements. Non-linear large deformation theory and a solid section type were employed. Following guidelines from previous reports [19], the mesh was generated with a minimum size of 0.1 mm and a maximum size of 3.0 mm. One end of the model was fixed in the longitudinal (x) direction, and a monotonic compressive load was applied at the other end in the same direction via forced displacement. Only one nodal point at the model's end was fixed in the cross (y) direction to prevent rigid body displacement. The entire model was subjected to an initial deflection in the orthogonal direction, calculated using Equation (1):

$$y_0 = \frac{a}{1000} sin \frac{\pi}{a} x y_0 = \frac{\mathrm{a}}{1000} \sin \frac{\pi}{\mathrm{a}} \mathrm{x} \quad (1)$$

Here, *a* represents the length of the specimen, and *x* denotes the distance in the longitudinal direction [20].

In the analytical model, the weld bead interconnected the base and patch plates. A rigid contact condition was assumed for the base plate surfaces and the inner surfaces of the patch plates, which could potentially come into contact underload. Residual stress was not considered in this analysis. The material constants used were Young's modulus of 206000 N/mm² and a Poisson's ratio of 0.3 for the steel components of the base plate, patch plate, and weld metal. As the mechanical properties of these elements varied in the experiment, the material properties consistent with the experimental conditions were applied in the analysis. Figure 7 displays the stress-strain curves of the steel materials, referencing models from a previous study [21]. These curves are derived from empirical formulas based on extensive experiments, allowing for accurate ABAQUS simulations.

3.2 Validation of the Analysis Model

Analytical and experimental results under static monotonic compression were compared to validate the analysis model. Figure 8 showcases the deformation of specimen F post-compression experiment as an exemplar. A comparison of the experimental and simulated deformations revealed general consistency, although not identical. This slight discrepancy could be attributed to the initial deflection in the simulations not precisely mirroring the actual conditions. Table 4 presents the simulation results under the same conditions as the experiment.

Furthermore, Figure 9 compares the load-displacement curves from the simulation with those obtained experimentally. It was observed that the experimental load-displacement curves for specimens A and D showed some differences from the simulated ones, likely due to smaller-than-expected weld bead sizes and experimental errors. However, the order of maximum loads for each specimen type was consistent, except for specimen E. As previously mentioned, specimen E exhibited incomplete root fusion, resulting in a smaller weld bead size and a reduced equivalent throat thickness compared to the anticipated 7.5 mm. This discrepancy likely affected the maximum load capacity of specimen E. The simulation results corroborated this, indicating that specimen E would have had the highest compressive strength without welding defects. Figure 10 displays the simulation result for specimen E with welding defects, using parameters discussed in section 2.3.2. The simulation confirmed that the welding defects decreased the maximum load capacity of specimen E, and the simulated curves closely aligned with the experimental results.

Thus, the feasibility of the analytical model, simulated using two-dimensional elastic-plastic analysis, was roughly verified. Excluding instances of mismatched actual weld bead sizes and welding defects, this analytical model can accurately analyse the maximum compressive strength for varying weld sizes, patch plate thicknesses, and lengths and evaluate their impacts.

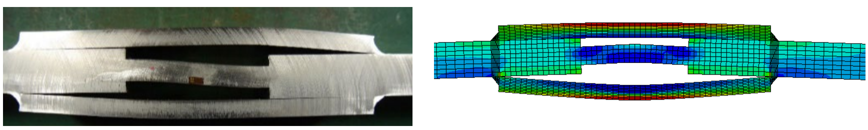

(a) (b)

Figure 8
The deformation of specimen F after the compression test: (a) Deformation photograph after the compression test; (b) Simulation result after the compression test

Table 4
Maximum loads of experiments and simulations (kN)

Type	A	B	C	D	E	F
Experiment	153.87	196.45	180.45	148.45	175.59	178.36
Simulation	172.18	189.81	185.75	166.96	192.52	182.88

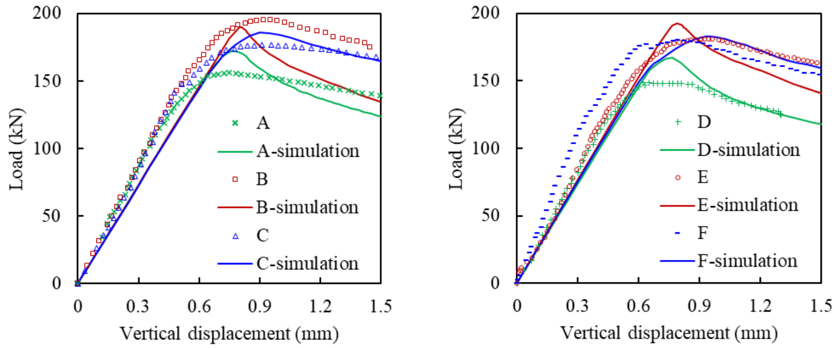

Figure 9

Load-displacement curves of simulation results: (a) Specimen A, B, C; (b) Specimen D, E, F

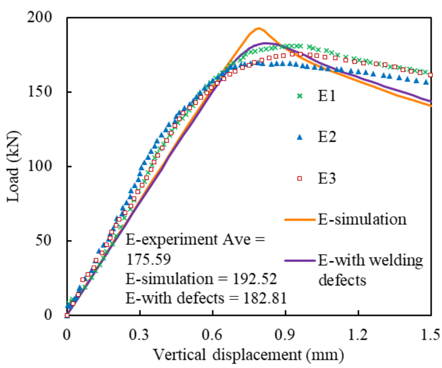

Figure 10

Simulation result of specimen E with welding defects tress-strain curve of steel materials

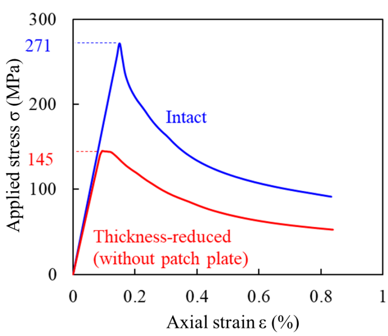

Figure 11

Stress-strain curves of intact and thickness-reduced (50%) models

3.3 Simulations with More Parameters

Building on comparisons between experimental and simulation outcomes, the roles of weld bead size, patch plate thickness, and length in patch welding repairs were confirmed. However, as mentioned in section 2.3, accurately measuring their impact on repair effectiveness requires more extensive simulations with broader parameter ranges. Thus, a comprehensive set of simulations was performed, exploring weld bead sizes from 4.5 mm to 9 mm, which correspond to t_w/d_c ratios of 0.71, 0.94, 1.02, 1.18, and 1.41 for sizes of 4.5 mm, 6 mm, 6.5 mm, 7.5 mm, and 9 mm, respectively. Patch plate thicknesses ranged from 4.5 mm to 9 mm and lengths from 60 mm to 180 mm. These simulations included 75 different models, with each configuration detailed in Table 5.

An intact model simulation was performed to determine this target stress level, as depicted in Figure 11, which shows both the intact and thickness-reduced models in ABAQUS and the resulting maximum stress. Figure 12 displays simulation results for varying parameters, with the target stress marked by a dotted line to represent the maximum stress of an intact model without any modifications. For weld bead sizes of 4.5 mm and 6.0 mm (Figures 12(a) and (b)), no model reached the target stress regardless of patch plate dimensions. In contrast, some configurations with a 6.5 mm weld bead size met the target stress (Figure 12(c)), likely due to the throat thickness t_w (4.6 mm) closely matching the thickness reduction d_c (4.5 mm), which aids in effective stress transfer. For s = 6.5 mm, longer plates typically resulted in slightly lower maximum stresses, except for the L = 60 mm case. For weld bead sizes of 7.5 mm and 9.0 mm (Figure 12(d)), the maximum stress generally exceeded the target stress, except for L = 60 mm scenarios. When the thickness-reduced area r and the patch plate length L were equal (60 mm), the maximum stress fell short of the target due to insufficient fixation of the patch plate ends. This suggests that rotation at the base plate support (welded part at the boundary of the corroded part) leads to increased out-of-plane deformation and reduced load-carrying capacity. Figure 13 illustrates cases with patch plate lengths of 60 mm and 90 mm, each having a patch plate thickness t_p of 4.5 mm and a weld bead size s of 4.5 mm.

From the simulation results, key findings were as follows:

a) Influence of weld bead size: For repairing thickness-reduced steel members under axial compressive load via welding patch plates, the weld bead size emerged as a critical factor impacting the repair's effectiveness.

b) Importance of thickness: Both the weld throat and patch plate thicknesses need to exceed the amount of thickness reduction. However, once the patch plate thickness surpasses the weld throat thickness, its additional impact on repair effectiveness is minor. With a consistent weld bead size, increasing the patch plate thickness does not substantially enhance the compressive strength.

c) Role of patch plate length: The patch plate length should extend beyond the thickness-reduced area to prevent rotation at the patch plate ends. The patch plate's slenderness ratio significantly affects the repaired member's compressive strength. A relatively shorter patch plate (e.g., L = 90 mm) is preferable to ensure adequate restraint against end rotation.

However, these findings are not entirely conclusive, particularly in real-world scenarios where corrosion typically spans a broader area and presents varying degrees of severity. The simulations in this section were limited by fixed parameters for the depth of thickness reduction and the area of thickness reduction on the base plate (d_c = 4.5 mm, r = 60 mm). Thus, the relationship between weld bead size and depth of thickness reduction, as well as the relationship between patch plate length and the area of thickness reduction, were not fully explored. To simulate realistic corrosion conditions more accurately, further analysis is required with varying depths of thickness reduction and different sizes of thickness-reduced areas. This additional investigation will help clarify the specific effects of weld bead size and patch plate length on the efficacy of patch welding repair.

Table 5

Simulations with more different dimensional parameters (mm)

Weld bead size, s (Throat thickness, t_w)	t_w / d_c	Thickness, t_p	Length, L
4.5 (3.2)	0.71	4.5, 6.0, 6.5, 7.5. 9.0	60, 90, 120, 150, 180
6.0 (4.2)	0.94	6.0, 6.5, 7.5, 9.0	
6.5 (4.6)	1.02	6.5, 7.5. 9.0	
7.5 (5.3)	1.18	7.5, 9.0	
9.0 (6.4)	1.41	9.0	

Table 6

Parameters with a fixed thickness reduction range (mm)

Thickness reduction, d_c	Thickness reduction range, r	Bead size, s	t_w / d_c	Length, L
2.25 (25%)	60	3.5, 4	1.09, 1.26	60, 90, 120, 150, 180
4.5 (50%)		6.5, 7	1.02, 1.10	
6.75 (75%)		10, 11	1.05, 1.15	

Table 7

Parameters with a fixed thickness reduction (mm)

Thickness reduction, d_c	Thickness reduction range, r	Bead size, s	t_w / d_c	Length, L
4.5 (50%)	60	6.5, 7	1.02, 1.10	r + 0, 30, 60, 90, 120
	90			
	120			
	200			

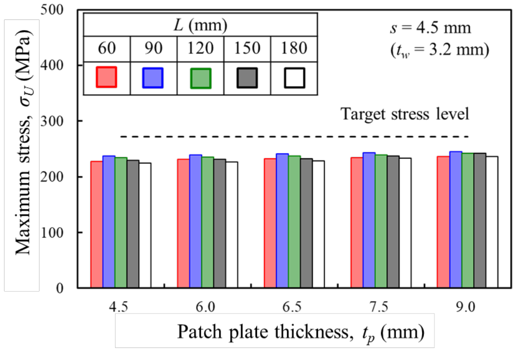
Maximum stress, σ_U (MPa)
L (mm)
60 90 120 150 180
s = 4.5 mm
(t_w = 3.2 mm)
Target stress level
0 100 200 300 400 500
4.5 6.0 6.5 7.5 9.0
Patch plate thickness, t_p (mm)

(a)

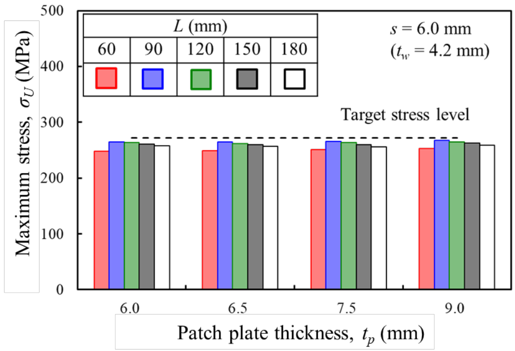
Maximum stress, σ_U (MPa)
L (mm)
60 90 120 150 180
s = 6.0 mm
(t_w = 4.2 mm)
Target stress level
0 100 200 300 400 500
6.0 6.5 7.5 9.0
Patch plate thickness, t_p (mm)

(b)

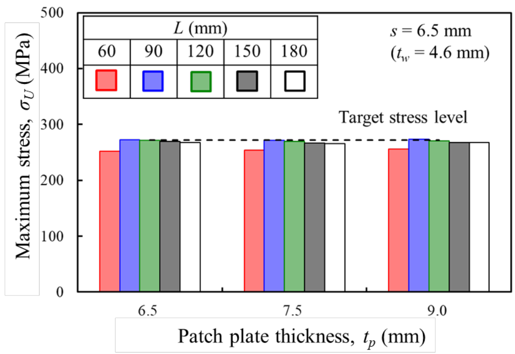
Maximum stress, σ_U (MPa)
L (mm)
60 90 120 150 180
s = 6.5 mm
(t_w = 4.6 mm)
Target stress level
0 100 200 300 400 500
6.5 7.5 9.0
Patch plate thickness, t_p (mm)

(c)

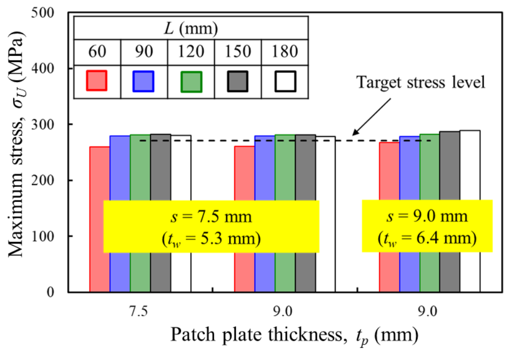

(d)

Figure 12

Patch-repair effects of the simulations with different dimensional parameters: (a) Bead size, s = 4.5 mm; (b) Bead size, s = 6.0 mm; (c) Bead size, s = 6.5 mm; (d) Bead size, s = 7.5 and 9.0 mm

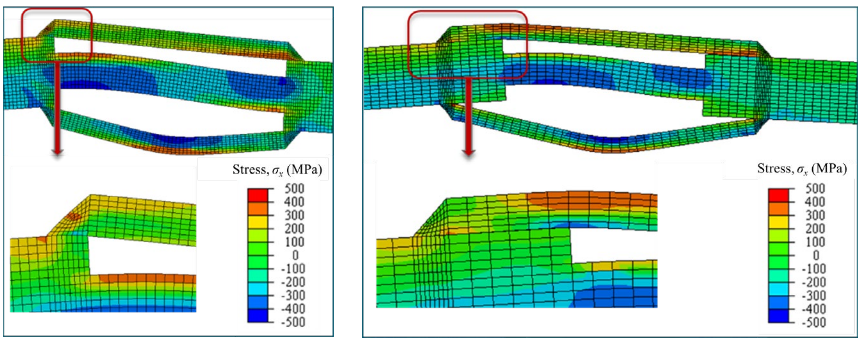

(a) (b)

Figure 13

Bending deformation after the compression test: (a) L = 60 mm, t_p = 4.5 mm, s = 4.5 mm; (b) L = 90 mm, t_p = 4.5 mm, s = 4.5 mm

3.4 Simulations with Different Thickness Reduction Depths and Areas

To better understand the effects of weld bead size and patch plate length on patch welding repair, a series of simulations were executed with varied thickness reductions and sizes of affected areas. These simulations built upon earlier findings that increasing patch plate thickness (t_p) beyond the weld bead size (s) offers only minimal gains in compressive strength. Therefore, in these simulations, t_p was set equal to *s*. Previous research [7] shows varying repair effectiveness across different corrosion levels, prompting simulations that ranged from mild corrosion (2.5% area affected) to severe corrosion (16.7% area affected). The simulations aimed to assess patch welding repair efficacy under various corrosion severities. Table 6 simulated three levels of thickness reduction—25%, 50%, and 75% (d_c = 2.25 mm, 4.5 mm, and 6.75 mm) with a consistent reduced area of 60 mm. Table 7 explored varying sizes of thickness-reduced areas—60 mm, 90 mm, 120 mm, and 200 mm, all with a fixed 50% thickness reduction (d_c = 4.5 mm). To ensure effective static stress transfer, the throat thickness of the weld bead (t_w) was maintained greater than the thickness reduction (d_c), with the tw/dc ratio exceeding 1, and in some cases, reaching 1.1. The length of the patch plate (*L*) was adjusted to span the reduced area (*r*) plus an additional 0 to 120 mm, resulting in 70 different models. This comprehensive approach is intended to yield clearer insights into optimal configurations for patch welding repairs across varying corrosion scenarios. The results of the analysis are depicted in Figure 14. The dotted line in the figure represents the target stress, which is the maximum stress of a model without any thickness reduction or patch plate. Models where the maximum stress with a welded patch plate surpasses this line indicate a restoration of compressive strength to a sound state.

a) Thickness-reduced area and throat thickness ratio: In scenarios where the thickness-reduced area (*r*) was 60 mm, and the ratio of the weld throat thickness (t_w) to the thickness reduction of the base plate (d_c) ranged between 1 and 1.1 (Figure 14(a)), the maximum stress did not reach the target stress. However, when r = 60 mm and the t_w/d_c ratio exceeded 1.1 (Figure 14(b)), the maximum stress attained the target level in all cases except where the patch plate length (*L*) was 60 mm.

b) Impact of patch plate length: The model with a patch plate length of 90 mm consistently showed higher maximum stress than other models, regardless of the thickness reduction. For a thickness reduction of dc = 4.5 mm and weld bead size of s = 6.5 mm (Figure 14(c)), the maximum stress fell short of the target. Conversely, for dc = 4.5 mm and s = 7 mm (Figure 14(d)), the maximum stress reached the target except when $L = r + 0$ mm and $r + 200$ mm. The most effective restraint against bending deformation occurred when the patch plate length was $r + 30$ mm, regardless of the length of the thickness-reduced area.

c) Bending deformation and contact: Bending deformation in a patch plate of length *L* results in contact with the base plate beyond the thickness-reduced area *r*. This contact restricts bending deformation. In our analysis, the optimal restraining effect was observed when $L = r + 30$ mm. Hence, setting the patch plate length to be about 30 mm longer than the thickness-reduced area, with a gap of approximately 15 mm between the fillet weld and the thickness-reduced area, is effective.

In conclusion, this section confirms that the ratio of weld bead size to thickness reduction depth for effective patch welding repair should be no less than 1.1.

Additionally, patch plate lengths extending beyond the thickness-reduced area by 30 mm demonstrated superior compressive strength compared to other lengths.

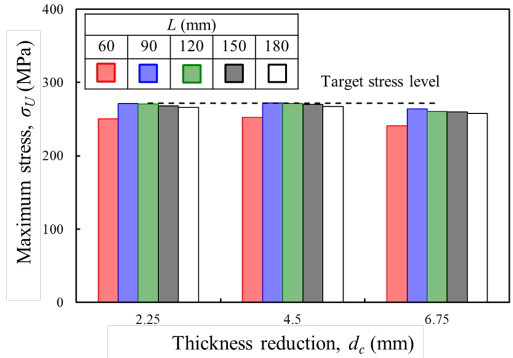

(a)

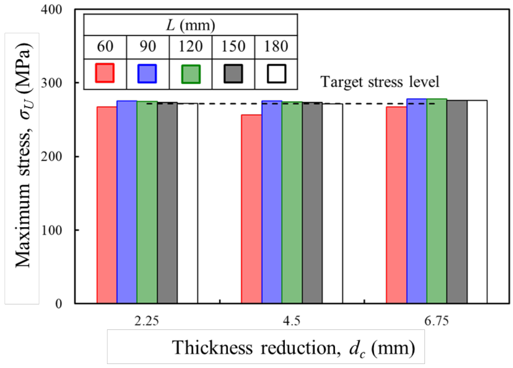

(b)

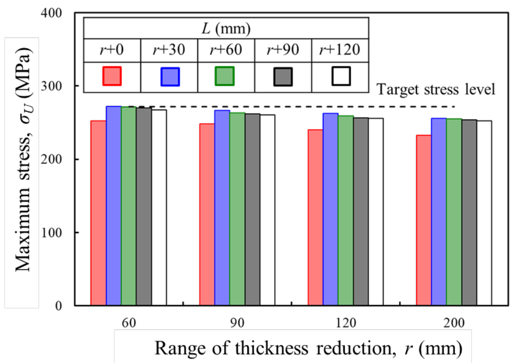

(c)

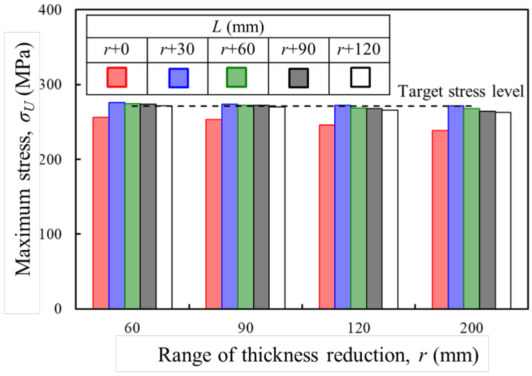

(d)

Figure 14

Patch-repair effects of the simulations with a fixed range of thickness reduction and fixed thickness reduction. (a) $r = 60$, $s = 3.5, 6.5, 10$ for $d_c = 2.25, 4.5, 6.75$; (b) $r = 60$, $s = 4, 7, 11$ for $d_c = 2.25, 4.5, 6.75$; (c) $d_c = 4.5$, $s = 6.5$; (d) $d_c = 4.5$, $s = 7$

Conclusions

This research conducted fundamental experiments and numerical simulations to explore the impact of patch welding repair on the compressive strength of steel members with corrosion-induced thickness reduction. The following conclusions were drawn:

1) Dominant Influence of Weld Bead Size: The weld bead size significantly influences the effectiveness of repairing thickness-reduced steel members under axial compressive load. The weld throat and patch plate thicknesses should exceed the thickness reduction, and the weld throat thickness-to-thickness reduction depth ratio is optimally greater than 1.1 in practical applications.

2) Patch Plate Thickness Impact: The impact of a patch plate thickness greater than the weld bead size on repair effectiveness is minimal. Increasing patch plate thickness without changing weld bead size does not substantially improve compressive strength. For cost-effectiveness, using a patch plate thickness equal to the weld bead size is recommended.

3) Patch Plate Length Requirement: The patch plate length must exceed the area of thickness reduction to effectively restrain end rotation.

4) Effect of Patch Plate Slenderness: The patch plate's slenderness affects the repaired member's compressive strength. Shorter patch plates are preferable for ensuring end rotation restraint. The optimal patch plate length is approximately 30 mm greater than the thickness-reduced area, with a recommended gap of about 15 mm between the fillet weld and the corrosion-affected area.

This study contributes to improving patch welding repair effectiveness and applicability for various patch plate dimensions. It aims to guide more cost-efficient patch welding repairs while ensuring the restoration of compressive strength. However, limitations exist in the current research. The assumption of uniform thickness reduction does not reflect the uneven nature of actual corrosion. Future research could involve more complex corrosion models to accommodate varying corrosion patterns longitudinally and transversely. Additionally, accounting for welding residual stress and the potential for structural failure due to localized corrosion, as suggested in previous studies [22], could be valuable for a comprehensive understanding of global and localized corrosion impacts.

Reference

[1] Farhey, D. N., Thakur, A. M., Buchanan, R. C., Aktan, A.E. and Jayaraman, N.: Structural deterioration assessment for steel bridges, Journal of Bridge Engineering 1997, 2(3), pp. 116-124

[2] Secer, M. and Uzun, E. T: Corrosion damage analysis of steel frames considering lateral torsional buckling, Procedia engineering 2017, 171, pp. 1234-1241

[3] Popoola, L. T., Grema, A. S., Latinwo, G. K., Gutti, B. and Balogun, A. S.: Corrosion problems during oil and gas production and its mitigation, International Journal of Industrial Chemistry 2013, 4(1), pp. 1-15

[4] Hirohata, M. and Fujimura, N.: Influence of thickness reduction in ase plate on elastic stress state of patch plate joint by combination of welding and bonding, Welding International 2019, 33(1-3), pp. 96-108

[5] Baker, A.: Fatigue studies related to certification of composite crack patching for primary metallic aircraft structure, In FAA-NASA Symposium on the Continued Airworthiness of Aircraft Structures, Atlanta, GA, Proceedings 1996, Vol. 1, pp. 313-330

[6] Morishita, T., Fujii, K., Morita, K., et al.: On rehabilitation of corroded steel plates by adhesive and steel cover plates, J Struct Eng A 2011, 57A:747-755

[7] Al-Hammoud, R., Soudki, K. and Topper, T. H.: Fatigue flexural behavior of corroded reinforced concrete beams repaired with CFRP sheets, Journal of Composites for Construction 2011, 15(1), pp. 42-51

[8] Takamori, A. and Amin, N. M.: Analytical study on cfrp repair method for lower flange of girder end with corrosion damages, Proceedings: Nurture Young Research Talent, 1st ed.; MNNF Publisher: Negeri Sembilan, Malaysia, 2020, 26-32

[9] Hollaway, L. C., Zhang, L., Photiou, N. K., Teng, J. G. and Zhang, S. S.: Advances in adhesive joining of carbon fibre/polymer composites to steel members for repair and rehabilitation of bridge structures, Advances in Structural Engineering 2006, 9(6), pp. 791-803

[10] Fu, Z., Wang, Q., Ji, B. and Yuanzhou, Z.: Rewelding repair effects on fatigue cracks in steel bridge deck welds, Journal of Performance of Constructed Facilities 2017, 31(6), pp. 04017094

[11] Pfeil, M. S., Battista, R. C. and Mergulhão, A. J.: Stress concentration in steel bridge orthotropic decks, Journal of Constructional Steel Research 2005, 61(8), pp. 1172-1184

[12] Hirohata, M.: Effect of joint dimension and restraint conditions on residual stress generated by patch welding, J Jpn Soc Civil Eng Ser A2(AM) 2016, 72(2):I_613-I_621 (in Japanese)

[13] Koch, G. H., Brongers, M. P., Thompson, N. G., Virmani, Y. P. and Payer, J. H.: Corrosion cost and preventive strategies in the United States, No. FHWA-RD-01-156, 2002

[14] Budhe, S., Banea, M. D. and de Barros, S.: Composite repair system for corroded metallic pipelines: an overview of recent developments and modelling, Journal of Marine Science and Technology 2020, 25(4), pp. 1308-1323

[15] Makabe, C., Naka, K. and Ferdous, M. S.: Method of arresting crack growth for application at a narrow working space, Mechanical Engineering Journal 2014, 1(6), pp. SMM0058-SMM0058

[16] Mori, H. and Hirohata, M.: Compressive behavior of steel cruciform column with thickness reduction repaired by patch plate welding, J.JSCE, Ser.A1 2020, 76(1), pp. 15-28 (in Japanese)

[17] Zmetra, K. M., McMullen, K. F., Zaghi, A. E. and Wille, K.: Experimental study of UHPC repair for corrosion-damaged steel girder ends, Journal of Bridge Engineering 2017, 22(8), p. 04017037

[18] Natori, Nishikawa K, Murakoshi J, et al.: Study on restrengthening of corroded steel bridge members, J Jpn Soc Civil Eng 2001, I-56(682), pp. 207-224 (in Japanese)

[19] Tanino, T., Ogata, H., Sakaida, K., et al.: A study on stress concentration factor on weld toes of cruciform welded joints by FEM analysis, J Jpn Soc Naval Architects Ocean Eng 2016, 24, pp. 309-315 (in Japanese)

[20] Japan Road Association: Specification for Highway Bridge Part II Steel Bridges, Maruzen Publishing Co., Ltd.: Tokyo, Japan, 2017 (in Japanese)

[21] Nakagawa and Suzuki, H.: Ultimate Temperatures of Steel Beams Subjected to Fire, Steel Construction Engineering 1999, 6(22), pp. 57-65 (in Japanese)

[22] Kainuma, S., Yang, M., Xie, J. and Jeong, Y. S.: Time-Dependent Prediction on the Localized Corrosion of Steel Structure Using Spatial Statistical Simulation, International Journal of Steel Structures 2021, 21(3), pp. 987-1003